Experimental study on the self-noise of a turbulent round jet investing a cambered aerofoil

Stefano Bianchi, *Alessandro* Corsini, *Anthony Geoffrey* Sheard

Abstract

This paper describes an experimental investigation of the interaction noise in a jet impacting isolated aerofoils. The authors conducted the study in a low-speed wind tunnel ending in an anechoic chamber, and focussed on the tip region of two types of isolated low speed axial fan cambered aerofoils. The authors set the Mach number, Reynolds number and blade incidence angles in a static frame of reference to reproduce a flow field condition kinematically similar to that in the rotating frame. They correlated far-field noise measurements with near-field pressure measurements which they took at different chord-wise positions in the blade's tip region. The aim was to find, by means of a cross correlation technique, a causal relationship between the aerodynamic sources in the tip region and noise emissions in order to establish the role of aerofoil self-noise associated with turbulent structures which turbulent inflow and blade tip geometry interaction produced.

Keywords

wind tunnel · chambered aerofoil · noise emission · turbulent structures

Stefano Bianchi

University of Rome Sapienza, Department of Mechanical and Aerospace Engineering, 18 Via Eudossiana, 00184 Roma,, Italy
e-mail: franco.rispoli@uniroma1.it

Alessandro Corsini

University of Rome – Sapienza, Department of Mechanical and Aerospace Engineering, 18 Via Eudossiana, 00184 Roma,, Italy
e-mail: alessandro.corsini@uniroma1.it

Anthony Geoffrey Sheard

Flakt Woods Limited, Colchester,
e-mail: geoff.sheard@flaktwoods.com

Nomenclature

Latin letters:

BPF	customary blade passing frequency of the fan rotor
c	blade chord position
f	frequency
L_p	sound pressure level of the cross spectrum (ref. 5 μPa)
St	Strouhal Number (fL/U_j)
SPL	sound pressure level of the auto spectrum (ref. 5 μPa)
U_j	jet average velocity
U_c	convection velocity

Greek letters:

α	blade customary angle of attack
α_L	wind tunnel correction factor of the angle attack
α_T	blade corrected angle of attack
γ^2	numerical value of the coherence function
λ_s	source length scale
θ	flow angle of deviation from the nozzle axis

1 Introduction

The research presented in this paper is part of an on-going noise reduction research stream aimed at developing the necessary technology to meet increasingly restrictive noise regulations and anticipated noise standards for low-speed axial turbomachinery. In particular, literature recognises the importance of the noise that originates from the interaction of unsteady disturbances at leading and trailing edges of an aerofoil, in fan or compressor blades, as a fundamental contributor to a rotor's overall acoustic emission.

The ingestion of turbulent flow sheared by aerofoil trailing or leading edges is a source of aerodynamically produced noise. Trailing edge noise has motivated scholars to study the problems associated with modelling the noise generation process. The acoustic analogy which Lighthill [1] developed stated that the turbulent fluctuations in the free space are inefficient noise radiators at low flow Mach numbers, due to the turbulent sources' quadrupolar-type character from which the radiated acoustic intensity through this region scales with the Mach number's eighth power. However, in the presence of a solid boundary, the sur-

face dipoles lead to a scaling with the Mach number's sixth power, as Curle [2] predicted and result in a louder noise. In the 1980s, Brooks and co-workers [3] studied an NACA 0012 aerofoil's trailing edge noise in a uniform free stream in a low speed wind tunnel. The study, in particular, speculated on the flow behaviour in the proximity of the blade surface. They classified five mechanisms responsible for the aerofoil self-noise generation, which differ in how the disturbances interact with the aerofoil.

This brief introduction provides an overview of the historical interest in the development of a physical understanding of the problem which a solid body invested by a steady flow presents. However, in practice, propellers and fans operate in non-uniform flow. When a turbulent eddy passes the edge of a solid body, the turbulent fluctuations radiate intensely, scaling with the Mach number's fifth power, as Fowcs Williams and Hawkings [4] showed. Therefore, due to this scaling, in the absence of other noise-generating mechanisms, the trailing edge and the tip gap are the most significant aerodynamic noise sources, especially at a very low Mach number. In static tests, researchers have deduced that the dominant noise component arises from the interaction between ingested turbulence and the rotor blades, as Magliozzi and co-authors [5] demonstrated. These researchers worked to develop an understanding of the physical mechanisms that are responsible for the noise associated to a solid body and an unsteady flow.

Blake and Gershfeld's past research [6] indicates that one potential source of both tonal and broadband noise is associated with ingested turbulence. The inflow turbulence can be of atmospheric origin, or caused by inlet duct and casing boundary layers. In the latter situation, which mainly contributes to the rotor noise emission, the turbulent inflow's interaction with the blades' tip region is more critical because of the higher peripheral velocity and flow incidence. Tip vortex noise is a rotor self-noise mechanism which contributes to rotor broadband noise. Marcinowski [7] first suggested the importance of tip noise in low speed fans, where tip shape changes influenced the high frequency broadband noise. Subsequently, Lowson [8] confirmed that increases in broadband noise levels occur with increasing tip clearance, with the largest increases being apparent at frequencies higher than the blade-passing frequency.

If the noise frequency remains high compared to the rotational frequency, the noise generation in a rotating blade in a turbulent flow is similar to that of an isolated aerofoil. The time and space variations of the incidence angle lead to loading fluctuations on the blade. If the length scale of the turbulence is such that one blade chops a given eddy, i.e. higher than the blade section thickness, the noise is usually broadband, whilst we normally associate dipole noise with the flow velocity scale's power, e.g. 'v6' velocity dependence. According to the aero-acoustic analogy, the random elementary surface pressure field's fluctuations around an aerofoil correspond to dipolar sources. These sources result also from coherent vortices impacting on rigid surfaces and are usually concentrated on the leading edge (Fedala *et al.* [9]; Magliozzi *et al.* [10]).

The basis for the extension of the rectilinear motion theory to rotational motion is that as long as the acoustic frequency is somewhat greater than the rotational frequency, we can ignore the rotational effects and treat the blade as an aerofoil in rectilinear motion at each instant of time. Researchers base this approach on the isolated aerofoil's linearised aerodynamic theory (Blake and Gershfeld, 1989). The far-field noise, which an aerofoil radiates, is related to the turbulent velocity field by transfer function which is independent of the aerodynamic flow characteristics. We can determine them for an isolated aerofoil and can apply them to rotating blades. The only limitation in this case is that this measurement technique neglects the blade aerodynamic interaction with other blades. Winkler *et al.* (2007) first proposed this approach for the trailing edge noise study of a highly cambered NACA five digit aerofoil at zero degrees angle of attack, with and without a boundary layer tripping (Roger and Moreau [11]).

Several studies have investigated the tip region's trailing edge noise. Kendall [12] measured the noise at the tip of a stationary aerofoil using a directional microphone system. George *et al.* [13] were the first to articulate a physical model of the tip noise mechanism. Looking at the interaction between turbulence and an isolated aerofoil, Amiet [14, 15] performed an extensive comparison with experiments on NACA aerofoils in rotorcrafts. Similarly, Brooks and Marcolini [16], and Brooks *et al.* [16], attempted to correlate the noise that stationary aerofoil section models emanated with that of helicopter propellers.

From the acoustic standpoint, there are several possible sources in the tip region of a high cambered aerofoil invested by a turbulent flow:

- the jet-like clearance flow could generate sound when leaving the clearance region either directly or by interacting with the blade tip edge;

- the tip leakage vortex feeds the unsteady perturbations into the blade wall pressure field that could become sound sources as the tip edge and/or the trailing edge corner scatters them;

- to these pure self-noise sources, one could add possible interaction noise sources due to ingestion of incoming disturbances by the tip clearance flow.

Recently, Grilliat and Jacob [17] discussed these findings for both aerodynamic and acoustic results of a single high cambered aerofoil experiment. Among the experiments concerned with tip clearance noise, Ganz *et al.* [18] careful study indicated that fan tip noise is not a significant sound source, although their study also illustrated that it is quite difficult to identify the role of tip clearance noise among other noise sources on a representative fan rig. Other studies on rotating rigs led to different conclusions as to the magnitude of tip clearance noise (Fukano and Jang, [19]; Fukano *et al.* [20, 21], and some even tackled the problem

Stefano Bianchi, Alessandro Corsini, Anthony Geoffrey Sheard

of tip flow control (Corsini and Sheard, [22]; Khourrami and Choudari [23]).

In this context, the objective of the present study is to isolate the effect of the interaction between the turbulent flow, produced by a round jet, and the blade tip of a high cambered aerofoil pertinent to industrial fan applications with a view to the effects on the noise emission. Similar to the aforementioned cascade experiments, the authors did not consider the rotation of the blade since they mounted the aerofoil on its proper impeller and froze any rotation. However, the authors corrected the inflow's relative angle in order to consider the rotating blade's kinematics and the actual loading conditions. The authors took the near-field surface measurements of the aerofoil's wall pressure in both pressure and suction side on ten different chord-wise positions in the tip region. They then correlated the near-field pressure to the far-field noise and attempted a causal relationship between the noise sources and the pressure fluctuations on the aerofoil surface. The far-field measurements were taken in the fully anechoic chamber with the medium at rest. The authors based this approach for the far-field measurements, following Winkler *et al.* [25], on the linear aerodynamic and acoustic theory of isolated aerofoil and extended it to a finite span blade's interaction with a fully turbulent jet. Concerning the correlation technique, the authors adopted the approach standard in the turbomachinery practices which Mongeau and co-authors [24] first introduced, and extensively used in successive works on subsonic jets and subsonic speed axial fans.

2 Methodology

The authors tested the aerofoil in the core of a round free jet blowing into an anechoic chamber, (Fig. 1a). They blew the jet through a circular nozzle at the end of a convergent duct onto the aerofoil. They aligned the jet's upper part 50 mm from the fan's inlet bell-mouth edge which blew the jet centreline approximately to the blade's tip region (Fig. 1b and Fig. 1c). The round jet's relative position to the blade assured an aerodynamic behaviour as close as possible to the rotating conditions. The authors used two microphone types for the far-field and the near-field measurements. They obtained the measured time series from positioned probes, to give an acceptable trade-off between signal-to-noise ratio and directivity according to Winkler *et al* [25] and Bianchi *et al* [26].

The far-field microphone was a free-field standard Bruel & Kijaer 1/3" protected with a foam ball. The microphone was located in the anechoic chamber 1.2 fan diameters off the blade trailing edge, with an angular anomaly $\theta = 30$ degree from the jet plume's centreline as recommended by Bianchi *et al* [27], Winkler *et al* [25] and Leggat and Siddon [29]. The probes in the near-field unsteady pressure measurements on the blade surface are GRAS Type 40PS surface microphones (Fig. 2, designed for measurements on planar and curved surfaces. These probes are 2.8 mm thick, with a useful frequency range up to 20 kHz and a dynamic range topping at around 136 dB. The authors acquired
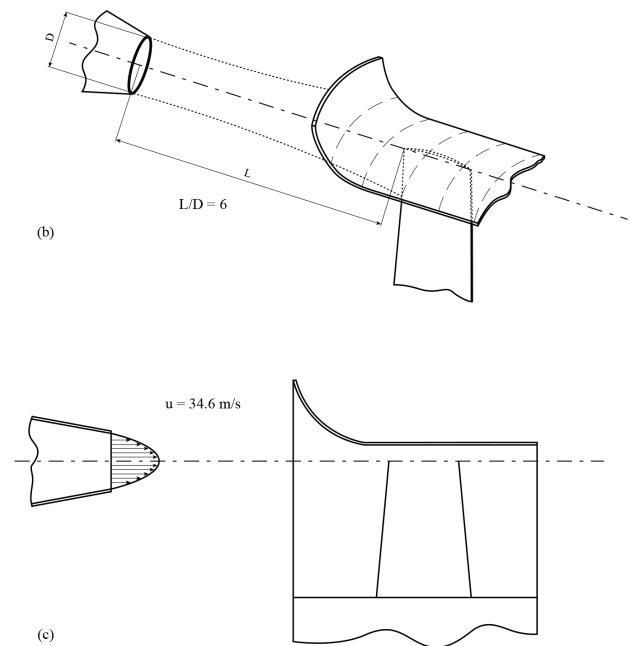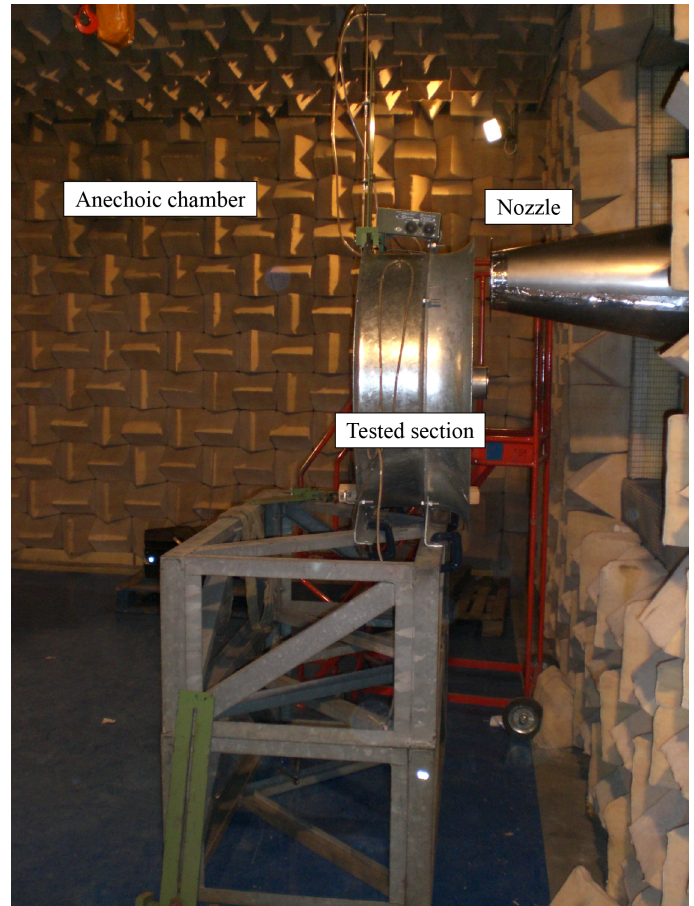
Fig. 1. Picture and schematic arrangement of a) the test rig, b) and c) the sector rig (not to scale).

all the microphone signals using a dBFA-AREVA Symphonie acquisition card.

The authors used the near- and far-field signals to compute auto- and cross-spectra. They obtained all the spectral data with 3.125 Hz bandwidth.
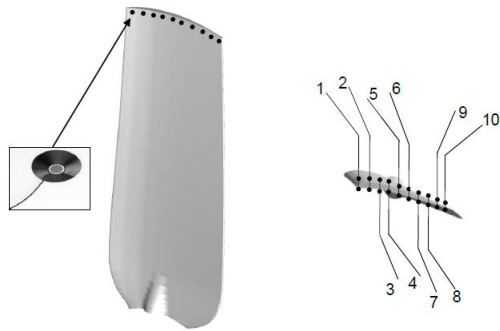
Fig. 2. Near-field set up of the pressure transducers (numbers represent the chord-wise probes' positions)

2.1 Aerodynamics characterisation of the round jet

The authors conducted the experiments in a round jet (Fig. 1 with an exhaust velocity of $U = 34.6$ m/s. The nozzle passage length/diameter ratio was $L/D = 6$. The dynamic pressure at the nozzle exit was 0.75 kPa and the static pressure 101.31 kPa. The Reynolds number at the nozzle exit was $Re = 5.15 \, 10^5$ and the relative Mach number was $M = 0.12$. The flow was fully turbulent at the jet exit and along the plume, confirmed by means of hot wire measurements.

The wide use of jets in experiments has led to many characterisations of jet flows, investigating thoroughly the effects of jet orientation, nozzle diameter and Reynolds number. To mention but a few, Ashforth-Frost and Jambunathan [30] as well as Cornaro *et al* [31] have published comprehensive reviews. Whilst providing valuable information on the jet flow's aerodynamic characteristics, researchers conducted all these studies for low Reynolds numbers and small nozzle diameters. These geometric and kinematic jet characteristics are comparable with the jet characteristics that the authors used in the present experimental study. The authors determined that the bulk of the flow is self-similar and depends on the momentum flux at the nozzle and on the fluid's viscosity and density. The reported literature indicates that researchers typically used the nozzle's width to reduce these data, but was not related to similar considerations which Narasimha *et al* [32] had already suggested. The authors verified the applicability and universality of the 'outer scaling law' (i.e. Coles' law of the wake [33] for the purposes of this paper, throughout the jet walls inviscid inner portion. In spite of this, the authors could not derive the logarithmic velocity distribution by making the usual assumptions based on Reynolds stresses or on the logarithmic region's relative thickness relative to the inner layer. They measured it using a hot wire anemometer previously located at the nozzle exit and traversed along the nozzle diameter.

2.2 Aerofoil section of the blades

The aerofoil under investigation is representative for a fan blade section which the engineers had previously developed and which the authors refer to as the blade configuration. In the present study, the authors compare the blade configuration to a blade with a fitted tip end-plate of variable thickness (TF*vte*) developed as a design solution for passive noise control (Corsini *et al*) [34]. The blade under scrutiny are illustrated in Fig. 3

The blade in the tip region was a modified ARA-D 6 per cent aerofoil, British Aeronautical Research type D for subsonic tip propellers. Tab. 1 provides the fan's specifications and aerofoil section. Concepts developed to control tip vortex and reduce induced drag in aircraft wings originally inspired the improved blade-tip configuration of the TF*vte* class of fans. Researchers have used similar configurations as anti-vortex devices in catamaran hulls.

Tab. 1. ARA-D 6% air-foil characteristics

	AC90/6 fans	
Blade geometry	Hub	Tip
l/t	1.32	0.31
Pitch angle (degrees)	36	28
Camber angle (degrees)	46	41
Solidity	1.24	0.3
Fan rotor		
Blade number	6	
Blade tip pitch angle (degrees)	16-28	
Hub-to-casing diameter ratio ν	0.22	
Tip diameter (mm)	900.0	
Rotor tip clearance τ (% span)	1.0	
Rated rotational frequency (rpm)	900	

2.3 Investigated flow conditions

The authors investigated the aerofoil's likely use as a fan rotor blade, using angular settings customary of compact cooling fan units, 28 degree tip pitch angle. They conducted all the measurement campaigns assuming, that the fan load condition was equivalent to a 160 Pa static pressure rise. The authors introduced corrections in the impeller blade's angular setting and in the air speed to simulate the rotational effect on the static blade test rig. Bianchi and co-authors [35–37] generalised the correction technique, which Brooks and co-authors [16] developed for the NACA 012 aerofoil for application with other aerofoils. The following sub-section discusses these corrections.

2.4 Aerofoil aerodynamic corrections

Aerofoil testing in a finite-size jet plume causes flow deflection and downwash and effectively reduces the angle of attack, in a condition similar to that of a finite-size wind tunnel (Brooks and Marcolini). As anticipated above, the authors reinterpreted the aerofoil angle of attack to account for the blade rotation and to simulate the actual loading condition at the tip. This, in turn, allowed the authors to incorporate the finite aspect ratio influence on the formation of the tip vortex.

Stefano Bianchi, Alessandro Corsini, Anthony Geoffrey Sheard

The authors corrected the angle between the aerofoil and the incoming air stream according to Brooks *et al.* [16] method, developed when testing aerofoil model sections in a finite open wind tunnel. The testing configuration effectively featured a reduced flow deviation (and downwash deflection of the incident flow). Brooks *et al* [16] used the lifting surface theory to develop a 2D open tunnel correction factor for the angle of attack and camber. The authors had to modify the blade's angle of attack α in real operating conditions in the tunnel to retain a similar lift condition of the tested section as a function of the blade's relative dimension with respect to the nozzle height. Brooks and co-workers [16] introduced a correction factor λ that reads as:

$$\lambda = (1 + 2\sigma)^2 + \sqrt{12\sigma}$$

with:

$$\sigma = \left(\frac{\pi^2}{48}\right)\left(\frac{\ell}{H}\right)^2,$$

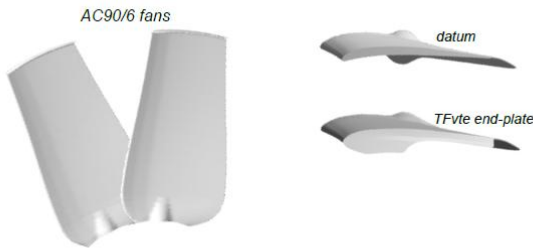where ℓ is the aerofoil chord and H is the nozzle height.

Fig. 3. Test fan rotor blades and tip end-plate, not to scale (Corsini *et al*)
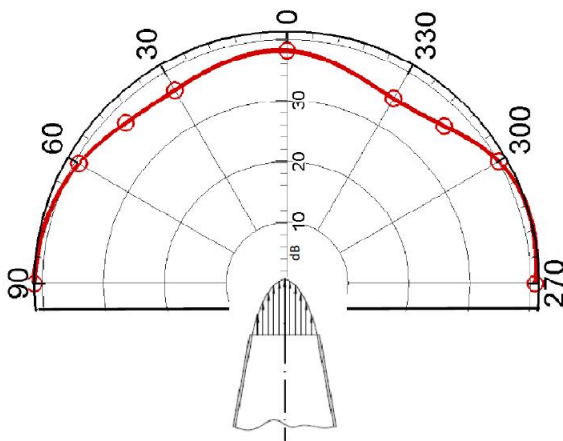

Fig. 4. Jet noise directivity plot (the symbols are in correspondence of the far-field microphone's position)

Using the factors from above, expressing the operative blade setting at the tip in terms of the tested fan's customary angle of attack, $\alpha = 6$, it was possible to calculate the corrected angular setting α_L, value to be added to the customary angle of attack,

with the expression: $\alpha_L = \lambda\alpha$. With $\lambda = 1.83$, the result in our case was $\alpha_L = 2.41$ degrees.

In this study, the blade in the rig had to simulate the effect of blade rotation with respect to the relative inflow kinematics. As the blade was not rotating, the boundary layer thickness reduced. The authors could avoid this phenomenon by recalculating the angle of attack of the static blade in the jet flow. Therefore, the authors applied a second correction factor to compute the blade's relative airspeed and angle of attack. As the fan rotates, the angle of attack and the flow speed vary along the span. The authors decided that they should investigate the flow behaviour and phenomena in the tip region. A low-speed jet designed to supply air in an annular region interesting the outer 30 per cent of the span. The authors avoided the jet shear layer's turbulent effect by placing the measurement section in the jet's inviscid core.

The authors developed a calculation method (Bianchi *et al*) [27, 35],in accordance with the above requirements, providing an estimate of the global angle (α_T) that considered both α_L and rotation effect. The authors calculated for a rotational speed of 900 rpm, which gave U_j 33 m/s, the corrected angle was $\alpha_T = 10.3$ for a corrected air speed at the tip of 34.7 m/s. The authors changed the blade pitch in the test rig using the calculated angular corrections.

3 Experimental Technique

The data analysis in this paper was derived from a comprehensive broadband noise experiment for stationary aerofoil developed by Brooks and Marcolini (1986) [3]. Testing parameters included flow average velocity, blade pitch angle, angle of incidence of the incoming flow and tip leakage flow control through a new aerodynamic tip end-plate geometric, compared with a impeller without tip enhancement. The authors present the experimental results 'as measured', whilst the theoretical aero-acoustics of the turbulence/aerofoil interaction include correction to account for the jet shear layer presence through which the sound must pass before reaching the far-field microphone. Note, that there were no adjustable parameters in the theory which the authors could have used to improve the agreement between theory and experiments for the tested aerofoil type.

The authors processed the instantaneous pressure data to derive quantitative data on the directivity of the tip noise and the influence of the tip modifications on human sound perception.

The authors recorded all measurements at a sampling rate of 50 kHz and used the Nyquist frequency at $f = 25$ kHz. To avoid signal aliasing, they filtered all data at 20 kHz and analysed it in the range below 20 kHz. The resulting Nyquist-rate was 2 kHz which was largely below the sampling frequency, thus verifying the second condition in the Nyquist problem on signal aliasing.

The authors estimated the overall uncertainty on unsteady pressure measurements as: i) $\Delta V = 1000$ mV 12 mV (20:1) on the voltage, and ii) Δ G= 200 dB 2.4 dB (20:1) for the row signal gain in the frequency ranges. The error in the Fourier

transform was in the range of 0.1-0.2 dB at 1 kHz and 2 dB at 10 kHz, as given by the calibration certification on the microphones and the acquisition system according to ISO IEC60651 (International Standard Edition, 2001–2012) [50].

3.1 Fourier analysis

The authors processed the auto- and cross-spectra using a signal post-process suite in the frequency range 25 Hz to 20 kHz with a constant bandwidth of 3.15 Hz. The digital signal processor acquired the signals from the far-field microphone and performed the cross correlation with the near-field blade surface pressure.

A transfer function that couples the pressure fluctuation (due to the unsteady flow in the near-field) with perceived noise in the far-field (which constitutes the response of the system) governs aero-acoustic emissions. Pseudo sound can degrade the results; however, in an anechoic chamber, the pseudo sound's transfer function has a shorter decay time than the same function transmitting the genuine noise emission to the far-field,Laurendeau *et al.* [42]. In accordance with Leggat and Siddon's [29] method, the authors chose the distance of the far-field probe from the fan as the optimum to avoid pseudo sound becoming coherent.

In the present study, the authors correlated the tip pressure measurements of the near-field with the measured noise at the far-field. In diagnosing acoustic sources, engineers find identification of the proper correlation domain useful for assigning flow regions in the near-field controlling the sound in the far-field. The cross-correlation between near- and far-field signals reveals a causal relationship between individual noise-source phenomena and the overall radiated sound in a given direction, thereby yielding quantitative information about acoustic source distribution, their local spectra and the scale of their coherence. If a strong harmonic coupling between a source in the near-field and far-field spectra exists, the resulting correlation function does not decay quickly, but is periodic in nature.

Thus, the authors derived a coherence function for the dataset. In accordance with Miles's suggested procedure (2006), the authors set the threshold for signal coherence at 95 per cent of the calibrated noise source and used this to confirm the anechoic chamber's acoustic performance. The authors used a white noise Brüel & Kjær Type 4204. This procedure ensured that only coherent sources contributed to the cross-spectra, whereas, the auto-spectra remained as a consequence of coherent and incoherent sources. Correlating near- and far-field data was a good solution for facilitating an improvement in pseudo sound correction.

3.2 The 'causality method'

The measurement of instantaneous pressure in the aerofoil near-field raises questions about the consequences of using such measurements to dissect noise-source activity. Measurements effected in the subsonic turbulent jet's near-field and rotating turbomachinery provide valuable information regarding the low-order dynamic flow (Bianchi *et al.* [35]; Laurendeau *et al.* [42]; Miles). Previous work has established that, in addition to the 'purely hydrodynamic' contributions, the near-field also comprises an 'acoustic' component related to the progressive pressure fluctuations put towards the reach of the far-field (Bianchi *et al.* [35]; Laurendeau *et al.* [42]; Ribner [39]).

Several studies on subsonic jet noise have reported on near-field pressure measurements under similar velocity gradients to those in the outflow from a fan rotor (Laurendeau *et al* [42]). With regard to the relationship between the near-field pressure and noise-source dynamics, Ribner [39] observed that the first-order approximation of the Lighthill source term is formally related to the pressure Laplacian in incompressible flows. Moreover, Laurendeau *et al* [42] have noted that the spectrum in the near-field combines a low frequency range dominated by the aerodynamic signature and a high frequency range that senses acoustic-pressure fluctuations. Recently, Bianchi and co-authors [27] used the same technique to correlate the near-field pressure, measured at the trailing edge region in a rotating low speed axial fan, and the far-field noise. The pressure in the near-field senses both the 'aerodynamic cause' and the 'acoustic effect' in different frequency ranges. Applied far-field filtering provides insights into the source-noise emission coupling mechanisms.

Building on the research reviewed above, this paper aims to correlate the local pressure fluctuations on the blade surface, measured for three chord positions in the tip zone, with the noise at the far-field measured in the different azimuthal angles which the experiments considered. This 'causality method' is no less than a high precision source localisation technique, which identifies the coupling mechanism's structure via which the largely redundant wall pressure dynamic drives the far-field pressure field.

The authors chose the position of the near-field microphones at ten positions along the aerofoil's chord to cover the three most important regions responsible for the tip noise emission: the leading edge (LE), the middle-chord region (MD) and the trailing edge region (TE). This is an important point given the aforementioned difficulty associated with identify the radiating part of a source in the near-field. As the formal identity between the source far-field correlation and the integral solution of Lighthill's equation, the filtering operation by which the said solution sorts and extracts acoustically matched source activity, is inherently present in the source far-field correlation. This is most effective, when the source fluctuation frequency matches with the far-field noise pressure. Other researchers have reported the same deduction in past studies on the jet noise source correlations (Jordan and Gervais) [40].

The second important consequence of using near-field pressure is that we are dealing with more than just the signature of a causal pressure dynamic. We also sense the beginnings of the acoustic response for certain frequencies, as the radiation extent of the aerofoil wall pressure field's 'hydrodynamic' component is a frequency function. The authors could sense low frequency

Stefano Bianchi, Alessandro Corsini, Anthony Geoffrey Sheard

'hydrodynamic' pressure fluctuations further in the aerofoil surface than the high frequencies due to their reflection on the rigid wall surface. The spectrum of the near pressure field thus comprises a low frequency range where perturbations are largely dominated by the hydrodynamic signature of the largest scale of the jet turbulence and a high frequency range dominated by progressive, acoustic fluctuations. So, the same near-field measurement senses both the cause and the effect in different frequency ranges. When we correlate them with the far-field measurements, which are sensitive only to the acoustic effects, it is possible to obtain valuable information related both to the mechanism by which the hydrodynamic cause couples with the far-field, as well as how the new-born far-field sound field at higher frequency radiates to the various far-field microphones. This also provides insight into the sound waves' directional character issuing from the aerofoil's rigid surface.

However difficulties exist concerning physical interpretation of the pressure field in this near-field region, and in particular when relating it to the sound production mechanisms. On the one hand, dynamics dominate the near pressure field which a linear hyperbolic differential equation best describes; whereas, it is essentially driven by a nonlinear hydrodynamic pressure field which is well approximated by elliptic equations. There is, however, a further difficulty related to the near-field's hyperbolic dynamics, and which hinders clear interpretation of near-field measurements. Nevertheless, together with the turbulence's hydrodynamic signature in the high rotational region, as it is for an aerofoil near the wall region, the near-field also contains the beginnings of a sound field which are destined to reach the far-field. As we are dealing with a jet investing an aerofoil, in addition to those discussed above, we have further complications which arise on account of the existence of different shear layers. We characterise these by different velocity gradients, turbulence scales and characteristic convection velocities.

Guitton et al [41] presented an empirical model which accounted for both, the different flow velocity dependence and the different spectral decay of the near-pressure field's hydrodynamic and acoustic components. They proposed the following criterion to predict the point at which we can observe transition from hydrodynamic to acoustic dominance.

Based on the above model, Laurendeau et al [38, 42] convincingly showed that for a jet flow with similar aerodynamic characteristics as the one the authors used in this measurement campaign, the transition region, of the hydrodynamic and the acoustic regime, lies somewhere in the region of $St = 1.3$ for a near-field to far-field microphone distance, equal to the one that the authors used in these experiments. With respect to the transition region's most amplified frequency, Laurendeau et al. [38] clearly indicated this value as $St = 0.7$. This means that, in terms of a cause-effect relationship, we seek to probe the limit of $St = 5$, imposed for the similarity of the static aerofoil's noise emission invested by a round jet with respect to a real rotating blade. This limited the value in understanding the

source dynamic details in providing information of the cause-effect regime, but informed on the directivity of the high frequency sound field emanating from the three locations at which the authors performed the near-field measurements. Nevertheless, this is strictly true for the cross-correlation analysis, as the tool of coherence analysis is still useful in order to highlight the cause-effect relationship. As the coherence function involves a normalisation by frequency band, it tends to highlight events that are highly coherent even if their energy is low, also inside the hydrodynamic regime. On the other hand, an analysis using the correlation coefficient, such as cross-correlation, will tend to suppress the low energy events and to highlight the effect-effect relationship that we associate with the most energetic events. The coherence analysis is better suited to highlight the near-field acoustic relationship to the far-field domain and gives a feel for the sound field's directivity that originates from different regions of the aerofoil tip. In addition, the cross-correlation analysis potentially provides information on the subtle details of the coupling mechanism via which the aerofoil wall pressure energy excites the far-field in a particular direction.

4 Discussion of the Results

The subject of the work is preceded by the analysis of bare test rig noise characteristics, where the authors explain the major limits of the measurements. The authors calculated spectral data resolving the L_p behaviours from the noise measurements on the blade with *datum* and improved tip end-plate configurations. The authors plotted the trailing edge noise's spectra as a function of the Stroual Number (St), with the frequency range limited between $St = 5$ and $St = 85$, in order to ensure the similarity of a frozen aerofoil noise emission with the real rotating blade noise emission.

4.1 Jet noise measurements

First, the discussion focusses on the test rig's sound characteristics to qualify the background noise due to the jet plume without the aerofoil's presence in the jet's core, but still with inlet case presence.

Fig. 4 shows directivity plot of the jet's overall sound pressure level SPL. As Fig. 4 illustrates, the authors could determine that the jet noise had a preferred noise emission path towards the closest positions of the jet side axis. Researchers did not recognise this finding for purely subsonic jets noise. In this kind of jet, the generated acoustic wave fronts originate mainly from the region where the mixing layers merge. Dominant sound sources are usually in the region near the end of the jet's potential core, in accordance with experimental observations (Bogey and Bailly [43]; Kandula and Vu) [44]. The authors attributed the difference to the presence of the inlet bell-mouth.

Fig. 5 illustrates a) the auto-spectra as measured 30 and 90 off the jet axis, and b) the coherence spectrum between the signals at 30 and 90. Fig. 5a shows the SPL auto-spectrum levels at 30 (blue line) and 90 (green line) angles. The trends of the levels

in the different positions were in quite good agreement, but two exceptions in the noise emitted at low St and in the St range comprised by $St = 30$ and $St = 55$. The experimental data for low frequencies (St 10) showed that the jet in this range radiated mainly toward the positions located in the jet's side-axis, i.e. 90. It is clear, that the inlet ring's presence mainly did not account for pure jet noise to get proper values, especially at a low St-number, but this was acceptable as the work focussed on the ducted aerofoil's noise emission, and then the authors considered the bell-mouth profile as a part of the test rig itself. The noise that the bare test rig emitted towards the position located closer to the jet axes, i.e. 30, was higher than the noise at 90 in the St-range between $St = 30$ and $St = 55$. This was probably due to the jet's pure turbulent mixing in the free space which generally produces broadband or narrowband noise at relatively high frequencies (Jacob *et al* [45]; Wang *et al* [46]).

Moreover, the authors calculated the coherence spectra between the two angular positions, in order to quantify the average coherence value of the rig background noise, and chose the appropriate threshold value in the aerofoil noise's successive analysis. Fig. 5b shows the coherence value was always lower than 0.2, apart from a few spots that were not higher than 0.28. For this reason, the authors set the coherence threshold at $\gamma^2 = 0.2$.

4.2 Aerofoil noise measurements

The authors applied the sequence of signal processing techniques, which the previous sections illustrated, to the pressure transducer signal located on the tip region's blade surface, and the far-field microphone noise signal. First, the authors analysed and commented on the considered aerofoils' geometry. After this, the results for the modified tip geometry (TF*vte*) are also discussed. The authors presented all the results in terms of directivity of the overall noise pressure level in the far-field, near-to far-field cross-correlation and coherence, calculated for the wall pressure which they took on both the aerofoil's pressure side (PS) and suction side (SS) in ten different positions along the chord, for the coherence calculations, and in three major positions for the cross-correlation: leading edge (LE), mid-chord (MD) and trailing edge (TE).

4.3 Datum aerofoil

As already discussed, the complexity of the experimental set-up makes it impossible to use Green's analytical functions tailored to the actual geometry. Moreover, the authors expected that the noise sources distributed along the aerofoil become non-compact around $St = 6$, thus a derivation of Green's function was practically impossible for the frequency range of interest. It is worth remembering, that the conventional *dictum*: '*correlation does not imply causation*' means that we cannot use correlation to infer a strict causal relationship between the variables. As the introduction explains, do not interpret this dictum to mean that correlations cannot indicate the potential existence of causal relations for an aerodynamically produced noise.

However, the causes underlying the correlation, if any, may be indirect and unknown, and high correlations also overlap with identity relations, where no causal process exists. For example, if the coefficient of the cross correlation is $r = 0.1$, as mainly occurs for the peak values in the emission of the studied aerofoil, then the coherence $\gamma^2 = 0.50$, which means that we can explain 50 per cent of the total variation in noise by the linear relationship between this noise and the aerofoil wall pressure (as described by the regression equation). The other 50 per cent of the total variation in the noise remains unexplained.

Bearing in mind the above stated limitations, the authors used cross-correlation and coherence analyses in their attempt to establish the causal relationship between the near-field wall pressure and the far-field sound domain. The far-field microphones were located 30 degree off the jet plume axis.

Fig. 6 shows the chord-wise map of near-to-far-field coherence (γ^2) in the *datum* fan blade. The noise measurements on the blade pressure side (PS), Fig. 6, indicate a significant coherence level distributed along the chord in a range of St up to 16. The coherence tones produced at the leading edge region (1 c 3), in the frequency range $St = 5$ to $St = 11$, are due to the flow impingement as a result of the inflow's turbulent nature affecting the structures of the flow/leading-edge interaction.

It is also possible to recognise γ^2 peaks appearing from the front to the blade's mid-chord, in coincidence with the positions where the flow leaking leads to the peak of leakage vortex rotational frequency. This observation is in agreement with past aerodynamic studies on the evolution of vortical structure in the *datum* rotor. This showed that the flow leaking occurred in the blade's front portion according to the relative clearance height and to the local load. From these experiments it drops off that, whilst all chord positions contribute to the noise sources in the frequencies $St = 5$ to $St = 7$ (with a higher $\gamma2$ value for $St = 5$), there are three chord-wise positions (namely $c = 4, 5 and 6$) that feature high coherence values of the noise sources radiated to the far-field. Probes at $c = 6$, $c = 7$ and $c = 8$ appear also to be relevant in the coherent sources of $St = 11$ and $St = 12$.

It is possible to generally distinguish that, in the *datum* aerofoil there are two phenomenon at play that constitute noise sources in the range of St <15. The first are the tonal sources characterised by a low St Number, mainly distributed along the whole length of the chord. These are related to both the leading-edge/flow interaction and tip leakage flow effects, which merge together, as causes of noise in the near-field, exciting the far-field with an effect which is mainly concentrated in the same frequency band. This is the resulting frequency of the merging sources (peaks observed at $St = 5$, $St = 6.3 - 6.8$ $St = 8$ and $St = 11$). In the noise emanating from a rotating aerofoil, we usually attribute this source to the loading effect. Recall, however, that the present experimental campaign did not include any correction for the loading effect, and so there should be no effects of unsteady noise loading. This observation leads the authors to attribute this source to the leading-edge turbulent gust
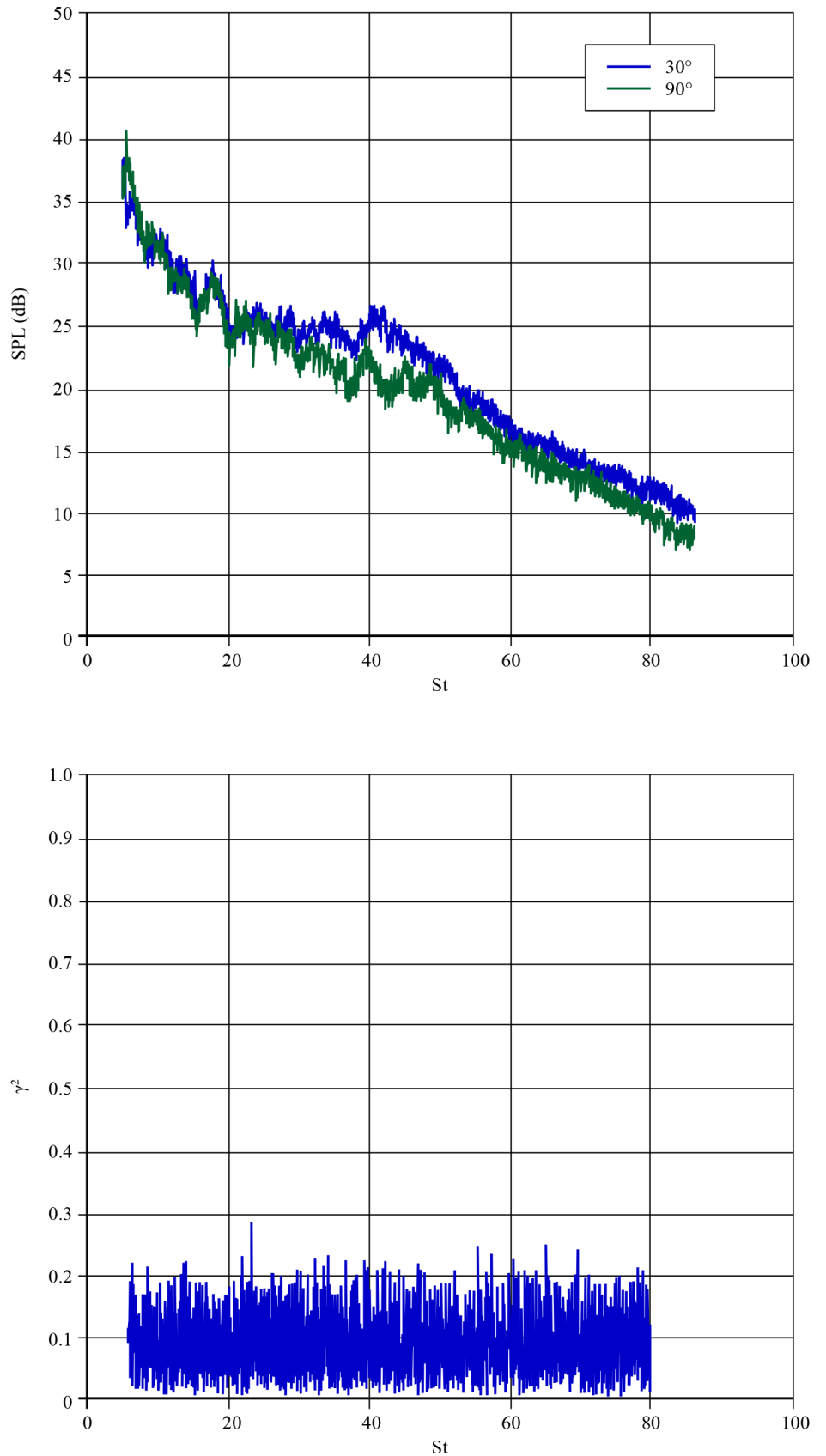
interaction. The second phenomenon at play originates from the sources excited by the leading flow's chord-wise evolution skewing around the aerofoil's tip region. Its effects in the far-field are visible at different frequencies: $St = 5.5$, $St = 6.5$, $St = 9$, $St = 10.8$ and $St = 15.2$.

As the frequency is higher than $St = 15$, the coherence spots are even more coarse as expected when the chaotic broadband noise sources became more relevant. Nevertheless, the
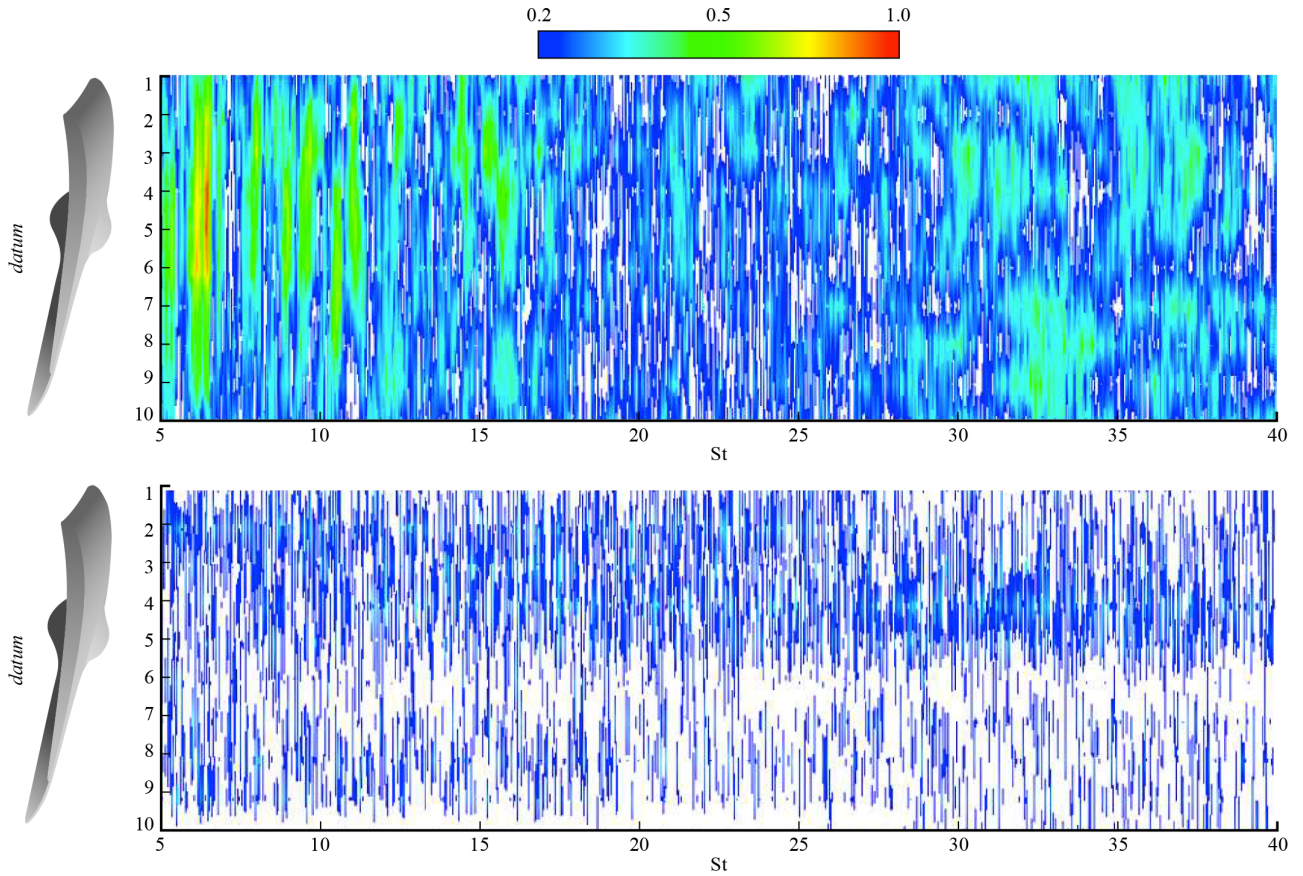
Fig. 6. Chord-wise map of near-to-far-field coherence function (γ^2) in the *datum* fan blade.
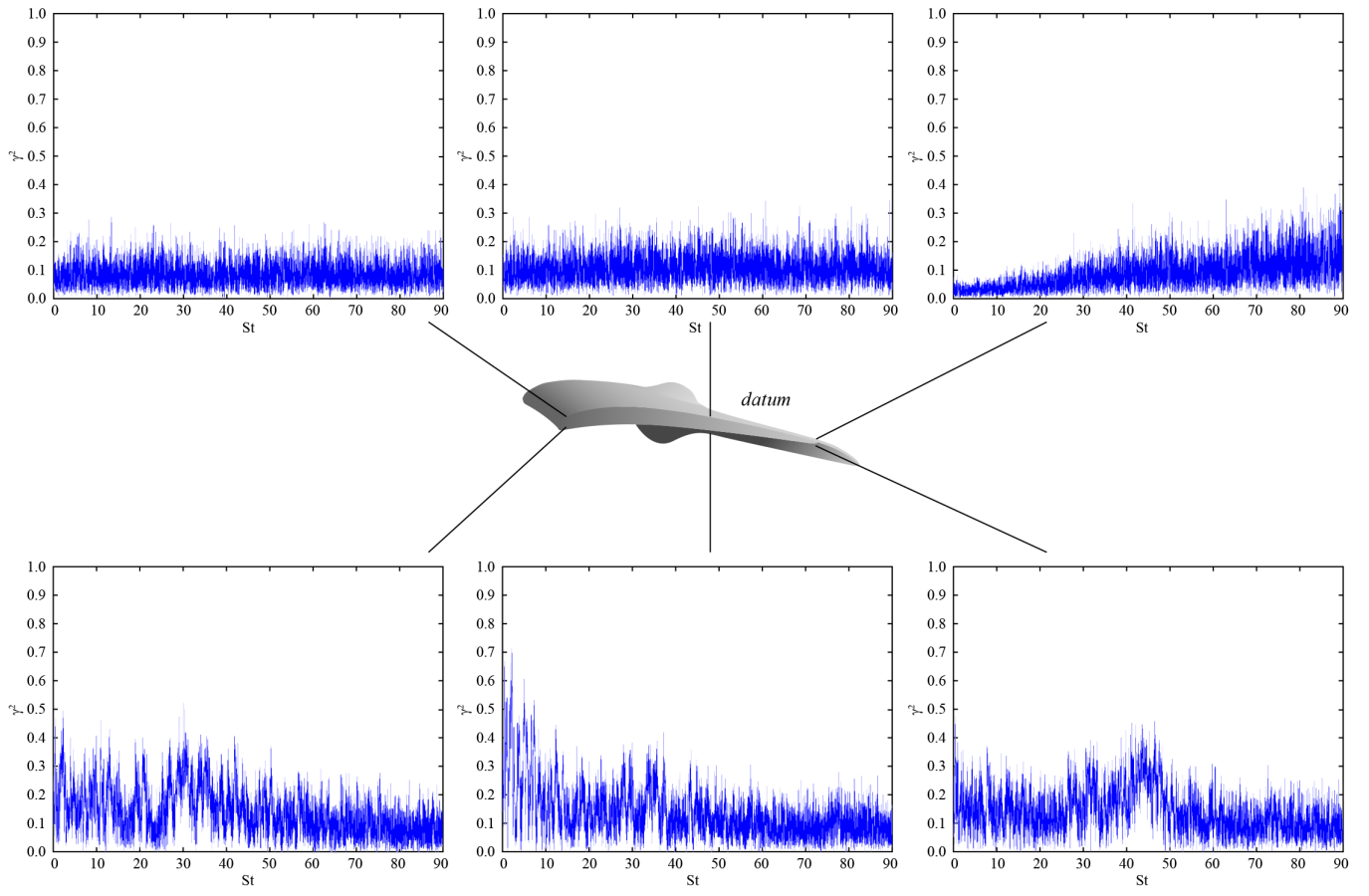
Fig. 7. Values of the *datum* aerofoil's coherence function (γ^2) at three different chord positions.

authors detected a group of coherent sources in $c = 1 - 5$ for $St = 31, 33, 36$ and 38. At $St = 33$ and 35, the coherent sources were localised in the proximity of the trailing edge ($c = 7 - 10$). Finally, a group of peaks in coherence appeared at $St = 35 - 40$, located part by the leading edge region and part by trailing edge, $c = 10$. It is possible to summarise that, in general, the *datum* geometry sees the low St-numbers sources ($St < 10$) correlated mainly to phenomena for which the aerofoil's leading edge region is responsible, whilst for $St > 10$, the noise appears to be excited by the tip leakage flow passage to the suction side towards the blade trailing edge, i.e. $c = 8 - 10$. Swirling flow interaction with the end-wall's boundary layers largely dominates these vortices. The authors interpreted this noise production mechanism in this range of $St > 30$ as trailing edge noise, as Fig. 6 depicts in the range $c = 8$ to 1, due to the passage of this turbulence over the edge and then into the wake.

On the *datum* blade suction side (SS), Fig. 6, the noise appears to be associated with development of leakage flow towards the blade trailing edge. The swirling flow's interaction with the end-wall's boundary layers again largely dominates this. In the stationary configuration it develops without forcing due to the end-wall drag. As the vortices' evolution produces a purely turbulent flow over the trailing edge and into the aerofoil's wake, a broadband nature characterises this noise that does not reach the analysis' threshold value in the suction side. This results in a spectral coherence map, which the absence of any relevant peak characterises. The suction side map appears clear of tones because the flow that excites the far-field is totally chaotic. The authors only observed two coherent strips, $\gamma^2 = 0.3$, in the proximity of position $c = 4$. This moderate coherent band existed for $St > 15$ up to $St = 40$.

For a deeper analysis of the relevant blade sources, Fig. 7 shows the discrete Fourier Transform of the coherence function plotted on St. The authors computed the coherence respectively, between the near-field wall pressure in three positions along the chord ($c = 1$ (LE), $c = 5$ (MD) and $c = 10$ (TE)) and the far-field probe. Fig. 7 illustrates the coherence spectra for both the *datum* blade sides (PS and SS). Notably, the far-field microphones are located 30 degree off the jet plume axis.

On PS at the LE ($c = 1$), we can characterise the coherence spectrum by one distinct peak region centred at $St = 7.5$ and a zone of smaller peaks from $St = 30$ to $St = 42$. At the MD position, the peak of coherence shifted towards the lower frequency, whilst the high frequency tones appeared at a reduced coherence. Moving towards the blade aft on PS, a distinct peak appeared centred at $St = 32$, that is probably the peak region's counterpart at 7.5 for the signal excited at the LE due to the ingested turbulence. The smaller peaks for $30 < St < 42$ at LE of excitation occurred over the same frequency range, and had a decreased coherence value. In general, the moving of a group of coherence peaks to higher frequency and the occurrence of other peaks in the same frequency range is an indication that the coupling mechanism's directivity is characterised both by a frequency selection mechanism, with the aerodynamic source characterised by a group of harmonics at low frequency that become gradually less efficient as we move from LE to TE, and a frequency modulation mechanism, as the signature's peak progression involved a shift to higher frequency as we moved from LE to TE (Laurendeau *et al*) [7].

On the blade LE, the near-field probe merged in the boundary layer and was sensitive to the oscillatory pressure field mechanism. We can associate this highly fluctuating source with the Kelvin-Helmholtz mixing-layer structure, which became less efficient as the near-field probe position approached the aerofoil's fully developed region. At 30 degrees TE, see Fig. 7, the frequency of the fully developed local turbulence of the boundary layer shifted to $St = 45$ and its strong signature were clearly evident. Apart from the expected components in the vicinity of the local mixing-layer frequency, there was an apparent, more efficient wavy coupling signature in the low St-values, represented by the smaller peaks for $5 < St < 10$ in LE and MD. The mentioned signature did not appear in the TE coherence, which the down-washed flow at $St = 45$ dominated fully. Laurendeau and co-authors also observed this frequency shift in a similar jet correlation, and they attributed this coupling mechanism's particular signature to two factors. The first is the possibility that for those frequencies, we are not yet out of the hydrodynamic field influence and so there is not a clean acoustic signature available. The second is that there may be an effect of non-compactness of the source. As the introduction stated, we can only consider the cause-effect signatures to translate a local pressure contribution to the far-field if the source is compact.

On the blade SS, the first observation is, that the coherence between the near-field probes and the far-field microphones at 30 degree in the suction side reveals a different trend, when compared with the measured coherence at the PS. For the radiation pattern at 30 degree, see Fig. 7, the coherence appears almost flat at $\gamma^2 = 0.2$ for the LE and the MD correlations. The coherence of the TE probe starts with a value of $\gamma^2 = 0.1$ in the low St-number region and then rises quite linearly to a value of $\gamma^2 = 0.2$ at $St = 40$. This finding supports in detail previous observations on the coherence maps (see Fig. 6). Additionally, we can attribute the general low coherence level in the SS zone, together with the flat shape for the 30 degree radiation, to less influence of the Kelvin-Helmholtz mixing-layer structure in the aerofoil side. These instabilities are not generally negligible in aerofoil SS, but the tip leakage vortex's turbulent evolution dominated the local noise production, which is chaotic in nature and hides all the other sources in what the authors of the present papers have called a 'turbulent shield'. The authors also observed this phenomenon in past noise absorption studies driven by the turbulence (Brown and Clifford), whereas the only frequency coupling mechanism is due to the tip leakage flow passing through the aerofoil tip gap.

Fig. 8 presents the coefficients of the cross-correlation functions derived from the near-field and the far-field signals at 30

degree. The presence of a peak often correlates with a perfect match of the two sets for the given near- to far-field time delay. The plots in Fig. 8 show the correlation coefficients in the time region from 3.4 $10^{-3}s$ to 3.8 $10^{-3}s$, which contains the peak value. As Miles (2006, 2009) recently demonstrated, the correlation coefficient's peak region in a near- to far-field cross-correlation is representative of different *cause-effect* and *effect-effect* mechanisms. The left side of the peak is determined by the direct correlated noise, which dominates the considered source and moves at acoustic speed along its full path to the far-field probe. (Miles (2009) dealt with the combustor pressure correlated noise in jet engines). The indirect aerodynamic noise controls the right side of the peak, which initially propagates with the mean flow velocity. Consequently, in Fig. 8 one might expect to see a correlation function with one smeared peak, due to the direct wall pressure noise, and a smaller smeared peak due to indirect aerodynamic noise. Proved, that the examination of the correlation functions of Fig. 8, the prior observation is generally the case.

When considering the *datum* aerofoil's SS, the analysis of the cross-correlation coefficients, see Fig. 8, also assists in dissecting the noise sources of interest. At the conditions of the proposed experiment, the authors could not clearly observe the *two-peaks phenomenon* in the cross correlation using the aerofoil surface pressure probes and the microphone at 30 degree in SS, as they could only observe one single peak for the LE and the MD cross-correlation coefficients, as Fig. 8 shows. Moreover, negative peaks followed the main peak when the correlated surface pressure probe was at the TE. The reason for only one single peak detection is not clear, but we may speculate on the basis of Miles' [49] analysis. Miles concluded it might be possible that a relative amount of indirect signal noise decreases when the detection occurs far from the mean flow preferential direction path, i.e. on the jet side. Another possibility is that the observed ripple is due to a convective entropy feedback mechanism which enhances only the direct aerodynamic noise in this case. However, in all other cases, the left peak is comprised of a positive and negative part. We observed two subsequent negative peaks running at about 0.004 $10^{-3}s$ delay time each, from the main positive peak. Here that the sign of the correlation coefficient respectively indicates the direction of the relationship, either positive or negative.

In order to enhance the analysis of this unexpected correlation function behaviour, Tab. 2 shows the resulting delay time of the peaks and their values for the pressure side. The results in Tab. 2 show that, as the chord position of the near-field probe tends to the TE, the successive peaks' time delays of the cross-correlation to the microphone at 30 degree are approximately constant, but the absolute peak values tend to increase, because of an indirect noise decrease and the consecutive direct noise increase due to the mixing-layer near the aerofoil surface.

We can obtain an interpretation of the results in Tab. 2, by looking at the time delay of each.

Tab. 2. Time delays and values at peaks of the cross correlation coefficients of the *datum* air-foil at PS.

	Time (10^{-3} s)	Peak
Leading edge	3.601	0.102
	3.603	-0.095
	3.605	0.038
	3.606	-0.2704
	3.609	0.0151
	-	-
Mid-chord	3.6	
	3.601	
	3.602	
	3.603	
	3.606	
	3.609	
Trailing edge	3.599	0.08
	3.602	0.118
	3.603	-0.076
	3.606	0.035
	3.607	-0.025
	-	-

Let define the time delay as

$$\Delta\tau\,(f_L)|_{peak} = \tau\,(f_L)|_{peak} - \tau_{ref}$$

where we calculate the time delay relative to a reference time τ_{ref} of 3.6 $10^{-3}s$, since all the peaks occurring in the cross-correlation are close to this value of propagation time delay (Tab. 2. Notably, we can obtain an estimate of the source's compactness by discussing the data in Tab. 2 and considering the shown correlation coefficients, in correlation with the jet's convection velocity, estimated as $U_c = 0.6U_j$. The characteristic time-scale, which corresponds to the correlation signature, is of the order of 3.6 $10^{-3}s$, thus providing a length scale of the order of $l_s = 0.15$ m. This length scale was computed by virtue of a convection velocity of 20 m/s, whilst the sound's wavelength at St comprised between 1 and 5 was 0.23 m λ0.12m. Therefore, the sources are clearly non-compact when we consider the entire wave envelope as the appropriate source length scale, and this constitutes a limit of the interpretation that the present work proposes. Appendix A discusses the consistency of the presented time delay calculations for this kind of flow.

Close examination of Fig. 8 shows some structure to the function with features that vary positively and negatively. As mentioned above, the plots show, that we cannot always observe two separate peaks at those cross-correlation positions with the PS microphones. It also shows the negative peak value which characterises the TE correlation's peculiar behaviour. When a single peak is present, we cannot always reliably determine a source separation of direct and indirect aerodynamic noise by the cross-correlation (Miles) [49]. However, the authors clearly identified a time delay in all cases, indicating the aerofoil surface pressure oscillation as the noise source. The plots representing the cross
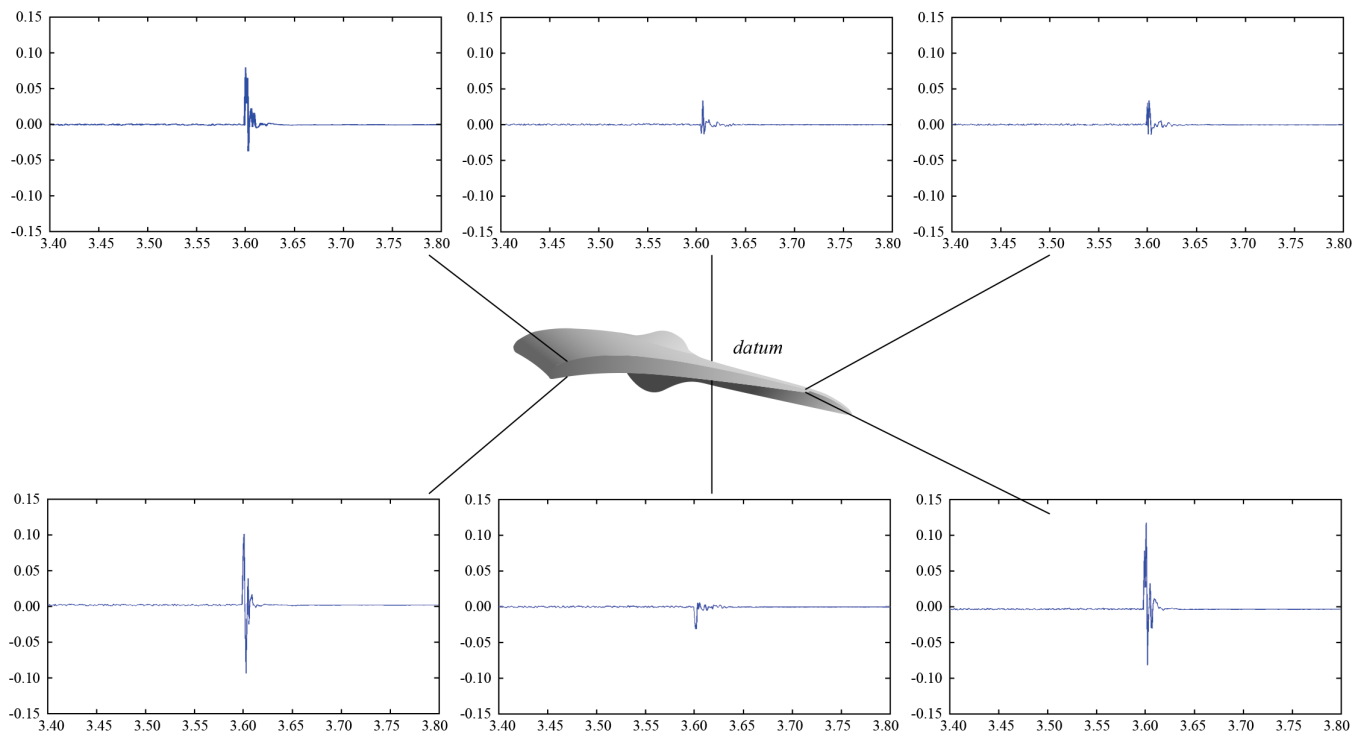
Fig. 8. The *datum* aerofoil's cross-correlation coefficients at three different chord positions.
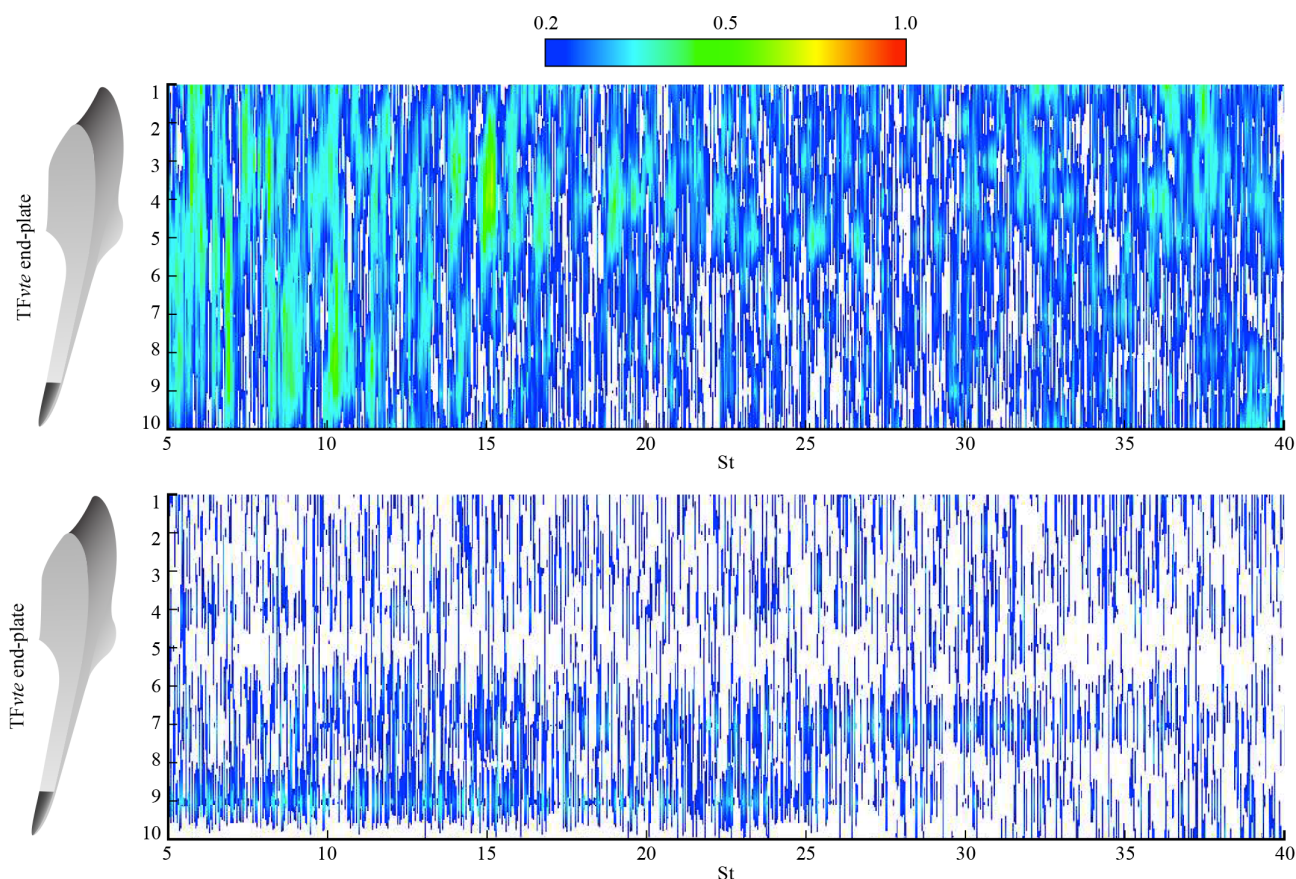

Fig. 9. Chord-wise map of near-to-far-field coherence function (γ^2) in the TF*vte* fan blade.

correlation with the noise radiated to 30 degree shows a unique peak at $3.602 \ 10^{-3}s$. It is clear, that some turbulent structure absorbed the correlated noise's negative peak in the LE region,

as occurred in the TE of PS. The region close to the TE is a zone of turbulence production, and many authors have reported excess noise attenuation due to the scattering by velocity fluc-

tuations on the turbulence's interaction with sound waves in jet noise (Miles) [49]. Consequently, the negative peak at the TE microphone might be due to more indirect aerodynamic noise, absorbed by the turbulent flow leaving the aerofoil trailing edge. The development of the leakage flow produced this turbulent flow, which swirling flow interaction with the end-wall's boundary layers largely dominated. If research peers accept the preceding analysis, the authors propose a further interpretation of the results. There is another mechanism of sound absorption: vorticity shedding from rigid surfaces (Bechert). Bechert [28] stated that the *Kutta condition* is crucial in this mechanism, as it is responsible for vorticity shedding and thus extracts energy from the sound field.

The vorticity shedding goes against the idea of an omni-directional, high frequency field radiated by what researchers sometimes associate with the 'fine-scale' turbulence. Questions arise from this observation and, even if we have supported this interpretation with similar observations derived from the turbulent jet noise, (Laurendeau *et al.* [42]; Tinney and Jordan [52]) the possibility that these frequencies are not entirely clear of the hydrodynamic field is still present, especially in the standard PS wall pressure conditions. For the same reason, the effect of the sources' non-compactness, discussed above, may compromise the analysis of the noise's cause-effect produced by sources located on the PS' aerofoil surface. This is a strong limiting factor associated with the authors' proposed interpretations. A more complete analysis, incorporating a quantitative method for establishing the extent of any cancellation effects which arise as a result of the sources' non-compactness, would require a more spatially extensive series of near-field measurements, both chord-wise and span-wise.

4.4 TF*vte* blade aerofoil section

The second element of the results which the authors present in this paper are an analysis of the noise sources in the blade's tip region with modified tip geometry (TF*vte*) and a discussion of the differences in the noise excitation, when we compare the results that the authors obtained with the TF*vte* geometry with the *datum*.

Fig. 9 shows the chord-wise TF*vte* coherence (γ^2) map. The authors detected the noise sources in the pressure side (PS). As Fig. 9 illustrates, the use of the coherence analysis now appears more chaotic. Nevertheless, the TF*vte* has a source distribution similar to the *datum* geometry. We can characterise this distribution by tonal and 'mainly coherent' sources, located in the low range of St, and by the absence of any correlated source in the frequencies of St >20. In spite of this, the tonal sources that the authors detected in the TF*vte* are less coherent than the sources that they previously found in the *datum*. All the tones excited by the *datum* in the range of $St = 5 - 15$ see a drop in coherence value: i.e. the tones at $St = 5$ and $St = 6 - 7$ are still present, but their coherence is now respectively $\gamma^2 = 0.3$ and $\gamma^2 = 0.4$, whilst in the *datum* the values were $\gamma^2 = 0.7$ for both.

The source at $St = 5$ has the same coherence level than in the *datum*. This is remarkable when considered within the context of the steady loading effects on the emitted noise. As the TF*vte* alters the aerofoil loading's chord-wise distribution, if this were important, then decreasing the steady loading would have had a different effect. Concerning the chord-wise distribution, there is a prevalence of sources localised in the first half of the chord. The coherent region's reduced extension (in terms of c and St) was in accordance with the control of secondary flows produced by attenuation of the near-surface fluid centrifugation, operated by this tip appendage. It is noteworthy that the TF*vte*'s highest coherent source is localised at $c = 4$ with $\gamma^2 = 0.7$. This geometry showed that the end-plate tapering by controlling the tip leakage vortex swirl was able to produce the occurrence of vortex instability onset in this position ($c = 4$) (Corsini *et al*). This instability facilitated the flow passage through the slot of the end-plate from PS to SS. Consequently, at $c = 4$ the local swirl augmentation resulted in a sound pressure instability that coupled with acoustic feedback to produce quasi-tonal noise.

When looking at the TF*vte* aerofoil's suction side (SS), see Fig. 9, the noise in the pressure side was mainly broadband in nature. The reason for the dominance of broadband noise was that the end-plate resulted in the creation of a system of vortical structures due to its scraping effect. The coherent strips in the *datum* are still present in the TF*vte*, but they have moved toward the TE, at $c = 7 - 9$. It is characteristic of this geometry that the tip vortex rolling onset and evolution probably related to the noise source presence (Bianchi *et al*) [41]. The coherence maps in Fig. 9 show, that the end-plate's presence governs the noise emission. This introduces an additional shedding mechanism that drives the radiated noise sources in a quieter excitation of the far-field. These observations provided evidence that the noise reduction mechanism that occurs with the TF*vte* end-plate configuration also occurs with the end-plate acting as a mixing enhancer in the tip-leakage region. The end-plate initiated an absorption caused by the vorticity shedding. We stress, that if there is a low St sound absorption in a rotating turbulent flow, which the authors' coherence causal analysis indicates, this is a linear effect. Furthermore, any broadband noise amplification does not compensate this linear sound energy loss. Such an effect does exist, but the 'clipping' of noise is a non-linear effect. Although studies on jet noise have experimentally shown, that an increased broadband noise follows rotating turbulent flow (Bechert), researchers have not yet proved that this mechanism exists in flow moving through blade rows.

The analysis of the coherence function, see Fig. 10, and of the cross-correlation's coefficients, see Fig. 11, in the three relevant chord positions ($c = 1$, $c = 5$ and $c = 10$), is again useful to understand the phenomena at play. The three positions' coherence functions, Fig. 10, confirm that the TF*vte* aerofoil behaves like the *datum* in both PS and SS. Moreover, Fig. 10 also highlights that although the shape is the same, the coherence value of the TF*vte* falls generally compared to the *datum* for all the consid-
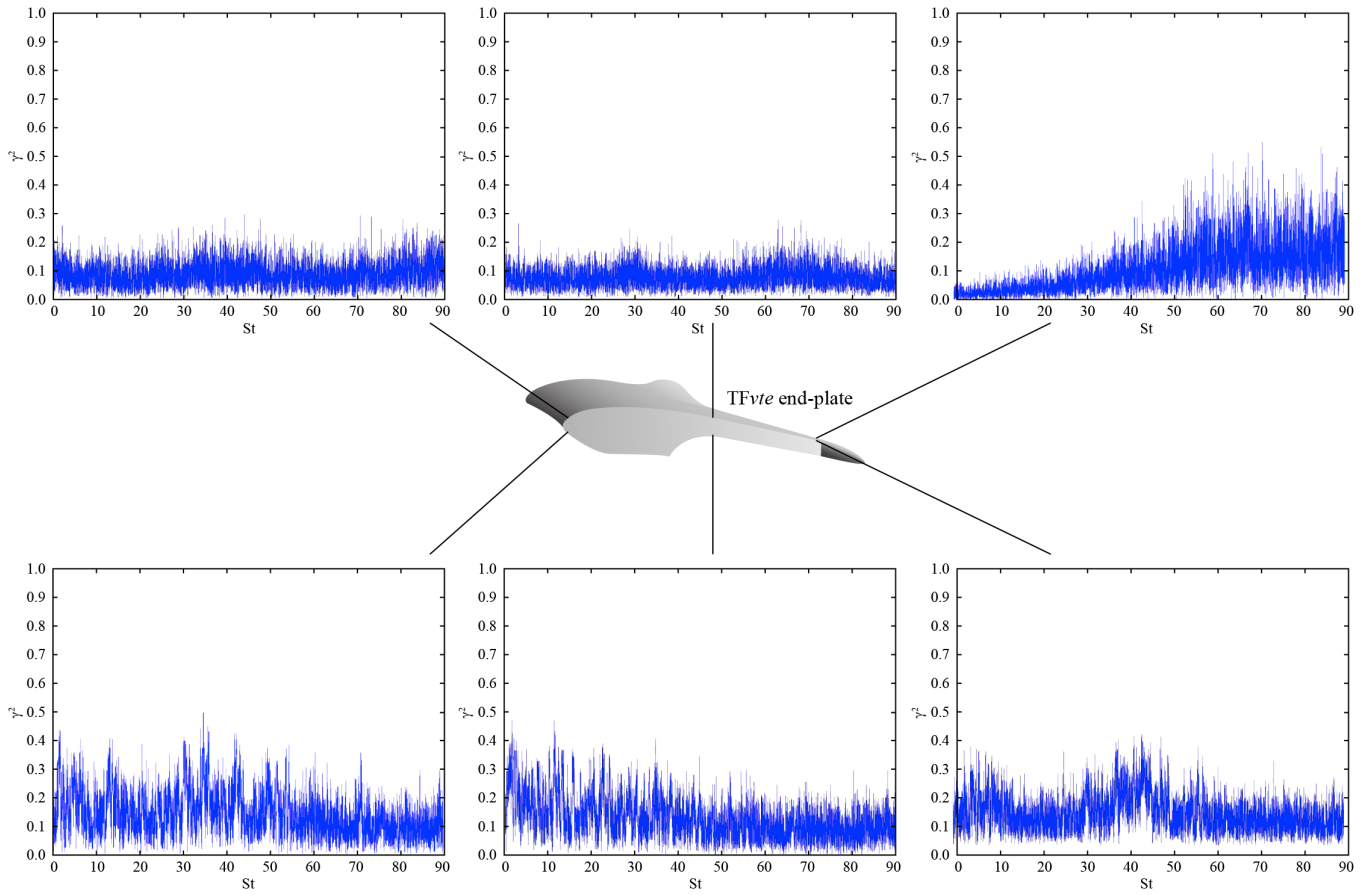
Stefano Bianchi, Alessandro Corsini, Anthony Geoffrey Sheard

Fig. 10. TF*vte* aerofoil coherence function (γ^2) values at three different chord positions.

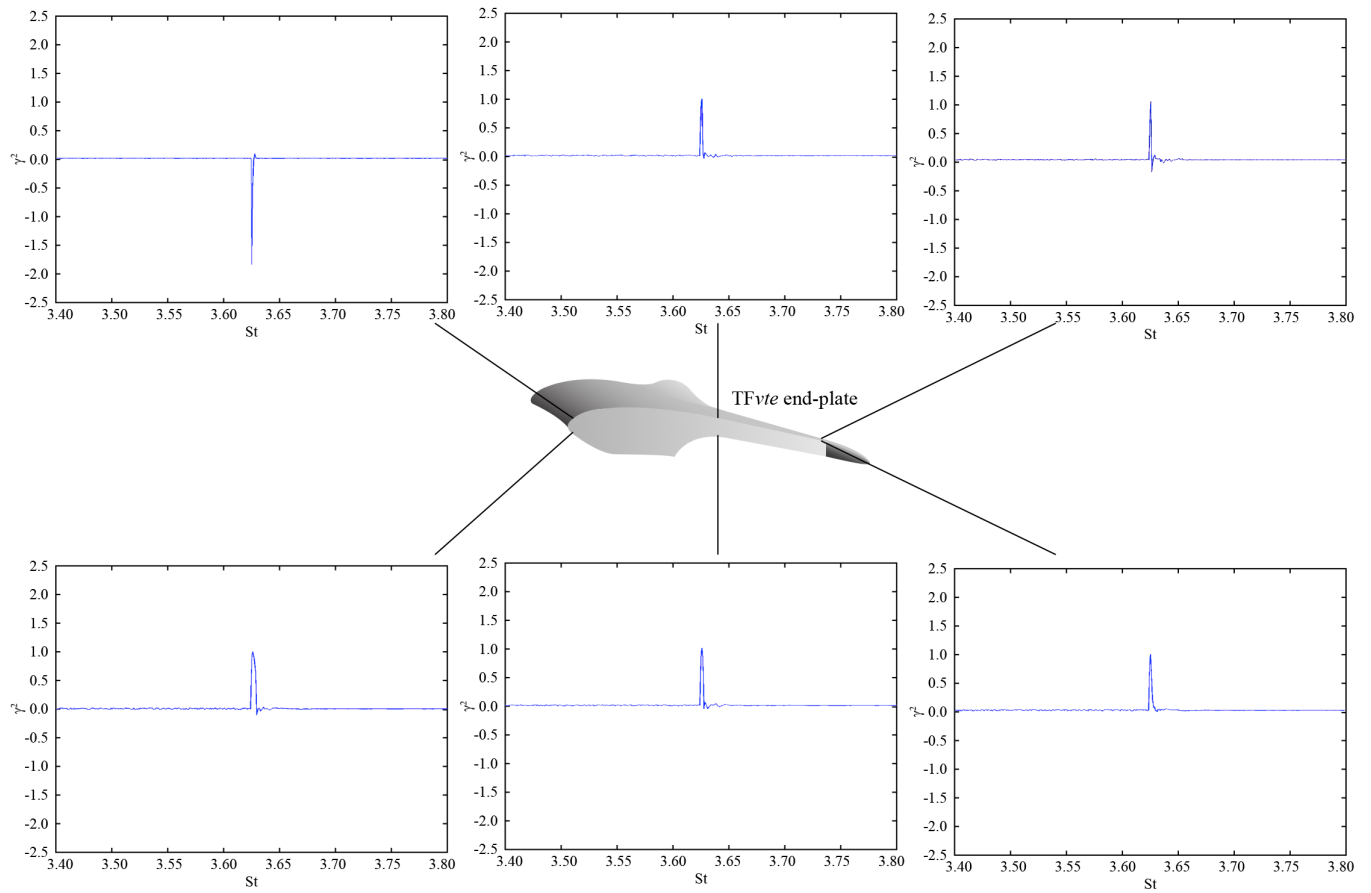**Fig. 11.** TF*vte* aerofoil cross-correlation coefficients at three different chord positions.

ered St ranges. Also, the TF*vte* values at low St are substantially cut off. This primarily occurs in the MD chord position of the PS. On the other side, the TE's 'quasi-linear' coherence rise reaches higher values due to the end-plate geometry's characteristic turbulence release.

The cross-correlation's coefficients, Fig. 11, show that the TF*vte* is characterised in both PS and SS by the 'one-only-peak' behaviour that the authors previously observed in the *datum* aerofoil's SS. As previously stated, the presence of a single peak does not allow the source separation of direct and indirect aerodynamic noise. From Fig. 11 we can infer that there is a clear absorption source which we can relate to the correspondent cross-correlation coefficient's negative peak at the TE of SS. The authors believe that the explanation for this behaviour may be that the end-plate's particular geometry in the stationary measurement acts as an additional noise absorption, i.e. separation or vortex shedding. On the basis of a dimensional argument, according to Fukano *et al* [21], the sound power level should linearly increase with the vortex scale, here in proportion to the gap height in the end-plate. The present measurements did not nearly increase with the vortex scale, because the absence of tip-to-casing relative motion significantly altered the momentum transfer within the gap. Moreover, the correction procedure acts on the aerofoil's actual tip region load. The lack of boundary layer flow centrifugation toward the casing annulus in the static sector rig resulted in blade tip loading, associated with not simulating rotation in the experimental programme which we report in this paper.

5 Concluding Remarks

The authors have experimentally investigated the change in the noise sources which two different aerofoils produce in a turbulent round jet and summarised the effect of the noise emission. We can use the calculation of the near- to far-field cross correlation coefficients and the analysis of a sequence of peak time delays and peak values to separate the type of the aerodynamic dependent source.

The cross-correlation function and the coherence function methods provided a procedure to detect the presence of coherent indirect and direct aerodynamic noise, when both are present. However, the inherent smearing of the cross-correlation that occurs as a consequence of the turbulence filtering renders difficult the determination of the indirect and direct noise's relative contribution to the total aerofoil noise.

The frequency of the fully developed *datum* aerofoil's local turbulence was $St = 32$. The components in the vicinity of the local mixing-layer frequency were at $St = 7.5$. We can associate this highly directional source with the Kelvin-Helmholtz mixing-layer structure, which became less efficient as the near-field probe position approached the aerofoil's fully developed region.

The authors do not interpret the large coherent peak occurring chord-wise for a St of about 5 as due to the aerodynamic

blade loading. Other than the effect of steady blade loading, the interpretation of the results is in agreement with other scholars' theories.

The modified geometry TF*vte*, when compared to the *datum* geometry, controls the coherent nature of the noise sources on the aerofoil wall in the tip region, acting as a mixing enhancer in the tip-leakage region, and provokes an absorption which the vorticity shedding causes. The most effective noise reduction method (assuming that one cannot reduce the tip gap) appears to be through tip flow control and the promotion of local turbulence which absorbs the noise emission and switching the harmonic sources to a broadband noise in the high frequency. Switching harmonic sources to broadband noise could offset somewhat the beneficial effect of decreasing the tip speed.

6 Appendix A – Delay Time Consistency

Based on Miles's research (2009), we can assume that the delay time of direct and indirect noise only depends on the difference between the entropy's travel time to the turbulent region's border that surrounds the aerofoil and the acoustic travel time to the same position. The authors ignored all other mechanisms that could impact on delay time in the present work. From the turbulent border to the far-field, the signals were acoustic and travelled the same path to the far-field microphone. We can estimate the delay time by:

$$\Delta\tau = \tau_s - \tau_a \approx L_j/v_j - L_j/c_j = \left(L_j/c_j\right)\left(1 - M_j\right)/M_j \approx L_j/v_s$$

whereas the difference in the measured time delay for the direct and indirect aerodynamic noise, $\Delta\tau$, was about $0.02 \ 10^{-3}s$, based on observing the cross correlation function coefficients. Reasonable values of M_j, L_j and v_s yielded values from $0.02 \ 10^{-3}s$ to $0.05 \ 10^{-3}s$ for $\Delta\tau$. The interesting point about the equation above is that the jet flow velocity mainly established the delay time and the jet core averaged diameter. Consequently, the time delay measured by the cross-correlation function should be fairly constant, regardless of the Mach and the jet characteristic length.

References

1 **Lighthill MJ**, *On Sound Generated Aerodynamically. II: Turbulence as a Source of Sound*, Proceedings of the Royal Society A:Mathemathical and phsyical engineering sciences, **222**(1148), (1954), 1–32, DOI 10.1098/rspa.1954.0049.

2 **Curle N**, *The Influence of Solid Boundaries upon Aerodynamic Sound*, Proceedings of the Royal Society A:Mathemathical and physical engineering sciences, **231**(1187), (1955), 505–514, DOI 10.1098/rspa.1955.0191.

3 **Brooks TF, Marcolini MA**, *Airfoil Tip Vortex Formation Noise*, AIAA Journal, **24**(2), (1986), 246–252, DOI 10.2514/3.9252.

4 **Williams JE, Hawkings DL**, *Sound Generated by Turbulence and Surfaces in Arbitrary Motion*, Philosophical Transactions of the Royal Society A, **264**(1151), (1969), 321–342, DOI 10.1098/rsta.1969.0031.

5 **Magliozzi B, Hanson B, Johnson DB, Metzge FB**, *Noise and Wake Structure Measurements in a Subsonic Tip Speed Fan*, **Report NASA**(CR-2323), (1973).

6 **Blake WK, Gershfeld JL**, *The Aeroacoustics of Trailing Edges*: **Professor Mohamed Gad-el-Hak** (ed.), Springer Berlin Heidelberg, 1989, pp. 457–532, DOI 10.1007/978-3-642-83831-6_10.

7 **Marcinowski H**, *Einfluss des Laufradspalts und der Luftfuehrung bei einem Kuehlgeblaese axialer Bauart*, Motortechnische Zeitschrift, **14**, (1953), 259–262.

8 **Lowson MV**, *Some Experiments on Fan Noise and their Implication*, Journal of the Acoustical Society of America, **52**(1A), (1972), 165, DOI 10.1121/1.1982011.

9 **Fedala D, Kouidri S, Rey R, Carolus T, Schneider M**, *Incident Turbulence Interaction Noise from an Axial Fan*, AIAA Paper No, (2006), 2006–2477.

10 **Magliozzi B, Hanson D, Amiet R**, *Propeller and Propfan Noise*, Aeroacoustics of Flight Vehicles: Theory and Practice, **Noise Sources**, (1991), 1–64.

11 **Roger M, Moreau S**, *Broadband Self-noise from Loaded Fan Blades*, AIAA Journal, **42**(3), (2004), 536–544, DOI 10.2514/1.9108.

12 **Kendall JM**, *Measurements of Noise Produced by Flow Past Lifting Surfaces*, Proceedings of AIAA Meeting, (1978).

13 **George A, Najar R, Kim FM**, *High-Frequency Broadband Rotor Noise*, Proceedings of AIAA 6th Aeroacoustic Conference, (1980).

14 **Amiet RK**, *Acoustic Radiation from an Airfoil in a Turbulent Stream*, Journal of Sound and Vibration, **41**(4), (1975), 407–420, DOI 10.1016/S0022-460X7580105-2.

15 **Amiet RK**, *Noise Due to Turbulent Flow Past a Trailing Edge*, Journal of Sound and Vibration, **47**(3), (1976), 387–393, DOI 10.1016/0022-460X7690948-2.

16 **Brooks TF, Pope D S, Marcolini MA**, *Airfoil Self Noise and Prediction*, NASA Publication, **1218**, (1989).

17 **Grilliat J, Jacob MC**, *Tip Leakage Experiment – Part One: Aerodynamic and Acoustic Measurements*, AIAA Paper, **No. 2007–3684**, (2007).

18 **Ganz UW, Joppa PD, Scharpf DF**, *Boeing 18-inch Fan Rig Broadband Noise Test*, **NASA CR-1998208704**, (1998).

19 **Fukano T, Jang C**, *Tip Clearance Noise of Axial Flow Fans Operating at Design and Off-design Condition*, Journal of Sound and Vibration, **275**(3–5), 1027–1050, DOI 10.1016/SO22-460X0300815-0.

20 **Fukano T, Kodama Y, Takamatsu Y**, *Noise Generated by Low Pressure Axial Flow Fans I – Modelling of the Turbulent Noise*, Journal of Sound and Vibration, **50**(1), (1977), 63–74, DOI 10.1016/0022-460X7790551-X.

21 **Fukano T, Kodama Y, Takamatsu Y**, *Noise Generated by Low Pressure Axial Flow Fans. II – Effects of Number of Blades, Chord Length and Camber of Blade*, Journal of Sound and Vibration, **50**(1), (1977), 75–88, DOI 10.1016/0022-460X7790552-1.

22 **Corsini A, Rispoli F, Sheard AG**, *A Meridional Fan*, Patent No. GB 2 452 104 B, (22 July. 2009).

23 **Khourrami MR, Choudari M**, *A Novel Approach for Reducing Rotor Tip-clearance Induced Noise in Turbofan Engines*, AIAA Paper No, (2001), 2001–2148.

24 **Mongeau L, Thompson DE, McLaughlin DK**, *A Method for Characterizing Aerodynamic Sound Sources in Turbomachines*, Journal of Sound and Vibration, **181**(3), (1995), 369–389, DOI 10.1006/jsvi.1995.0146.

25 **Winkler J, Temel FZ, Carolus T**, *Concepts, Design and Characterization of a Small Aeroacoustic Wind Tunnel Facility with Application to Fan Blade Measurements*, Proceedings of Fan Noise, **3rd Symposium**, (2007).

26 **Bianchi S, Corsini A, Rispoli F, Sheard AG**, *Near-field Aeroacoustic Experimental Investigation in Low Speed Axial Fans*, Proceedings of the American Society of Mechanical Engineers Noise Control and Acoustics Division NoiseCon2008, Dearborn, Michigan, 28th, (30th July 2008).

27 **Bianchi S, Corsini A, Rispoli F, Sheard AG**, *Experimental Aeroacoustic Studies on Improved Tip Geometries for Passive Noise Signature Control in Low-Speed Axial Fan*, ASME Journal of Vibration and Acoustics, **131**(6), (2009).

28 **Bechert DW**, *Sound Absorption Caused by Vorticity Shedding, Demonstrated with a Jet Flow*, Journal of Sound and Vibration, **70**(3), (1980), 389–405, DOI 10.1016/0022-460X8090307-7.

29 **Leggat LJ, Siddon TE**, *Experimental Study of Aeroacoustic Mechanism of Rotor-vortex Interactions*, The Journal of the Acoustical Society of America, **64**(4), (1978), 1070–1077, DOI 10.1121/1.382065.

30 **Ashforth-Frost S, Jambunathan K**, *Effect of Nozzle Geometry and Semi-confinement on the Potential Core of a Turbulent Axi-symmetric Free Jet*, International Communications in Heat and Mass Transfer, **23**(2), (1996).

31 **Cornaro CC, Fleischer AS, Goldstein RJ**, *Flow Visualization of a Round Jet Impinging on Cylindrical Surfaces*, Experimental Thermal and Fluid Science, **20**(2), (1999), 66–78, DOI 10.1016/S0894-17779900032-1.

32 **Narasimha R, Narayan KY, Parthassarathi SP**, *Parametric Analysis of Turbulent Wall Jets in Still Air Turbulent Incompressible Plane Wall Jet Flow in Still Air, Examining Maximum Velocity, Total Thickness and Inner Length Scale with Parametric Analysis*, Aeronautical Journal, **77**, (1973).

33 **Coles D**, *The Law of the Wake in the Turbulent Boundary Layer*, Journal of Fluid Mechanics, **1**, (1956).

34 **Corsini A, Rispoli F, Sheard AG**, *Shaping of Tip End-plate to Control Leakage Vortex Swirl in Axial Flow Fans, Transactions of ASME*, Journal of Turbomachinery, **132**(3), (2010).

35 **Bianchi S, Corsini A, Rispoli F, Sheard AG**, *Experimental Investigation of the Near-field Aero-acoustic Noise Sources of a Low Speed Axial Fan*, Proceedings of the XIX Biannual Symposium on Measuring Techniques in Turbomachinery, (7th–8th April 2008).

36 **Corsini A, Rispoli F, Sheard AG**, *Aerodynamic Performance of Blade Tip End-plates Designed for Low-noise Operation in Axial Flow Fans, Transactions of ASME*, Journal of Fluids Engineering, **131**(8), (2007).

37 **Corsini A, Sheard AG**, *Tip End-plate Concept Based on Leakage Vortex Rotation Number Control*, Journal of Computational and Applied Mechanics, **8**(1), (2007), 21–37.

38 **Laurendeau E, Jordan P, Delville J, Bonnet JP**, *Source Mechanism Identification by Near Field-far Field Pressure Correlations in Subsonic Jets*, International Journal of Aeroacoustics, **7**, (2008).

39 **Ribner HS**, *The generation of sound by turbulent jets*, Advances in Applied Mechanics, **48**(8), (1964), 105–182.

40 **Jordan P, Gervais Y**, *Subsonic Jet Aeroacoustics: Associating Experiment, Modelling and Simulation*, Experiments in Fluids, **44**, (2008).

41 **Guitton A, Jordan P, Laurendeau E, Delville J**, *Velocity Dependence of the Near Pressure Field of Subsonic Jets*, AIAA Paper, **2007–3661**, (2007).

42 **Laurendeau E, Jordan P, Delville J, Bonnet J**, *Nearfield-farfield Correlations in Subsonic Jets: What Can They Tell Us?*, 28th AIAA Aeroacoustics Conference, **AIAA Paper**, (2007), 2007–3614, DOI 10.2514/6.2007-3614.

43 **Bogey C, Bailly C**, *Investigation of Sound Sources in Subsonic Jets using Causality Methods on LES Data*, AIAA Paper, (2005), 2005-2885.

44 **Kandula M, Vu B**, *On the Scaling Laws for Jet Noise in Subsonic and Supersonic Flow*, AIAA Paper, (2003), 2003–3288.

45 **Jacob M, Boudet J, Casalino D, Michard M**, *A Rod-airfoil Experiment as Benchmark for Broadband Noise Modelling*, Theoretical and Computational Fluid Dynamics, **19**(3), (2005), 171–196, DOI 10.1007/s00162-004-0108-6.

46 **Wang M, Moreau S, Iaccarino G, Roger M**, *LES Prediction of Pressure Fluctuations on a Low Speed Airfoil*, Center for Turbulence Research, **Annual Research Briefs**, (2004).

47 **Brown EH, Clifford SF**, *On the Attenuation of Sound by Turbulence*, Journal of the Acoustical Society of America, **60**(4), (1976).

48 **Miles JH**, *Core Noise Diagnostics of Turbofan Engine Noise Using Correlation and Coherence Functions*, AIAA Paper, **2009-1237**, (2009).

49 **Miles JH**, *Procedure for Separating Noise Sources in Measurements of Turbofan Engine Core Noise*, NASA/TM-2006214352, (2006).

50 *International Standard ISO IEC 60651 and ISO IEC 61400-11*, **Edition 2001–2012**.

51 **Blake WK, Gershfeld JL**, *The Aeroacoustics of Trailing Edges, in Gad-el-Hak, M. (ed.)*, Frontiers in Experimental Fluid Mechanics, **46**, (1989), 457–532, DOI 10.1007/978-3-642-83831-6-10.

52 **Tinney CE, Jordan P**, *The Near Pressure Field of Co-axial Subsonic Jets*, Journal of Fluid Mechanics, **611**, (2008), 175–204, DOI 10.1017/S0022112008001833.